# Kv4 Channels Exhibit Modulation of Closed-State Inactivation in Inside-Out Patches

Edward J. Beck and Manuel Covarrubias
Department of Pathology, Anatomy and Cell Biology, Jefferson Medical College at Thomas Jefferson University, Philadelphia, Pennsylvania 19107 USA

ABSTRACT The mechanisms of inactivation gating of the neuronal somatodendritic A-type $K^+$ current and the cardiac $I_{to}$ were investigated in *Xenopus* oocyte macropatches expressing Kv4.1 and Kv4.3 channels. Upon membrane patch excision (inside-out), Kv4.1 channels undergo time-dependent acceleration of macroscopic inactivation accompanied by a parallel partial current rundown. These changes are readily reversible by patch cramming, suggesting the influence of modulatory cytoplasmic factors. The consequences of these perturbations were investigated in detail to gain insights into the biophysical basis and mechanisms of inactivation gating. Accelerated inactivation at positive voltages (0 to +110 mV) is mainly the result of reducing the time constant of slow inactivation and the relative weight of the slow component of inactivation. Concomitantly, the time constants of closed-state inactivation at negative membrane potentials (−90 to −50 mV) are substantially decreased in inside-out patches. Deactivation is moderately accelerated, and recovery from inactivation and the peak G–V curve exhibit little or no change. In agreement with more favorable closed-state inactivation in inside-out patches, the steady-state inactivation curve exhibits a hyperpolarizing shift of ~10 mV. Closed-state inactivation was similarly enhanced in Kv4.3. An allosteric model that assumes significant closed-state inactivation at all relevant voltages can explain Kv4 inactivation gating and the modulatory changes.

## INTRODUCTION

The somatodendritic subthreshold A-type $K^+$ current in neurons ($I_{KA}$) helps to control the frequency of slow, repetitive spike firing and acts as a shock absorber that prevents the backpropagation of action potentials (Connor and Stevens, 1971; Connor, 1978; Hoffman et al., 1997). Kv4 channels are important components of the $I_{KA}$ in the nervous system and also contribute to the $I_{to}$ current in cardiac myocytes, where they help to repolarize the early phase of the action potential (e.g., Serodio et al., 1994; Johns et al., 1997; Dixon et al., 1996; Song et al., 1998; Shibata et al., 2000; Malin and Nerbonne, 2000). The functions of these channels depend critically on the rates of development of inactivation and recovery from inactivation. However, the kinetic and molecular bases of Kv4 inactivation gating and how this process is modulated by various cellular factors are still poorly understood. Earlier reports have shown that low molecular weight (LMW) mRNA species from brain encode factors that enhance surface expression and accelerate inactivation gating of Kv4 channels (Chabala et al., 1993; Serodio et al., 1994, 1996). Kv4-specific $Ca^{2+}$-binding proteins that partly contribute to this modulation were recently identified (An et al., 2000). These proteins favor surface expression and remodel inactivation gating by a complex mechanism (Beck et al., 2001).

Several studies have investigated the modulatory mechanisms of inactivation gating in voltage-gated $K^+$ channels (Kv channels). One mechanism involves auxiliary $\beta$ subunits that introduce rapid N-type inactivation in Kv1 channels (Rettig et al., 1994; Pongs et al., 1999). Second-messenger pathways also mediate modulation of inactivation gating. Specifically, phosphorylation directly or allosterically modulates N-type inactivation in Kv3.4, Shaker D, and Kv1.4 channels (Covarrubias et al., 1994; Drain et al., 1994; Roeper et al., 1997; Beck et al., 1998; Antz et al., 1999). Another mechanism involves oxidation of the N-terminal inactivation domain of certain Kv channels (Kv1.4 and Kv3.4), which impairs rapid inactivation (Ruppersberg et al., 1991). Also, external pore residues apparently mediate modulation of C-type inactivation in cell-free membrane patches expressing Kv1.3 (Kupper et al., 1995). Finally, inactivation of certain Kv2 and Kv4 channels is modulated when they are coexpressed with "silent" $\alpha$ subunits (Jegla and Salkoff, 1997; Kramer et al., 1998). One of the main problems that has prevented a better understanding of the modulatory mechanisms of inactivation gating in Kv4 channels is the apparent absence of the N-type and C-type mechanisms that are namely responsible for the rapid and slow processes of inactivation in Shaker $K^+$ channels, respectively (Jerng and Covarrubias, 1997; Kirichok et al., 1998; Jerng et al., 1999). Novel mechanisms of Kv4 inactivation include the putative concerted action of the cytoplasmic N- and C-terminal regions of the pore-forming subunit (rapid inactivation) and putative interactions between the S4–S5 loop and the distal section of S6, two regions that contribute to the inner vestibule of the pore (slow inactivation). Although rapid inactivation in Kv4.1 channels may occur from the open state, slow inactivation

*Received for publication 23 October 2000 and in final form 3 May 2001.*
Address reprint requests to Manuel Covarrubias, Department of Pathology, Anatomy and Cell Biology, Jefferson Medical College at Thomas Jefferson University, 1020 Locust St., Philadelphia, PA 19107; Tel.: 215-503-4341; Fax: 215-923-2218; E-mail: manuel.covarrubias@mail.tju.edu.

0006-3495/01/08/867/17 $2.00

mainly occurs from a closed state and is coupled to channel closing at positive membrane potentials (Jerng et al., 1999). The latter means that the opening equilibrium is not strongly forward-biased in Kv4 channels and that final inactivation originates from the preopen inactivation-permissive closed state. Therefore, the rate of channel closing can indirectly influence the development of inactivation.

Here, we report that, upon patch excision (cell-free, inside-out (IO)), Kv4.1 and Kv4.3 channels expressed in *Xenopus* oocytes undergo significant acceleration of the development of macroscopic inactivation accompanied by a leftward shift in the voltage dependence of steady-state inactivation and an apparent partial rundown. These changes occur simultaneously and were reversible by the technique of patch cramming (Kramer, 1990; Costantin et al., 1999). We examined the consequences of these perturbations to investigate in detail the biophysical basis of inactivation gating in Kv4 channels over a wide range of membrane potentials (−140 to +110 mV). An allosteric state diagram that assumes significant closed-state inactivation (Klemic et al. 1998) at all relevant voltages can readily explain the major kinetic features of Kv4 gating and all changes induced by patch excision. The latter is solved by simply assuming that inactivation from the preopen closed state in IO patches is more favorable. The results also suggest that diffusible or labile cytoplasmic factors that preferentially modulate closed-state inactivation are present in intact native *Xenopus* oocytes. It is therefore conceivable that certain cellular factors encoded by the LMW mRNA from brain modify the endogenous modulatory factors and thereby influence inactivation gating of Kv4 channels. Also, an important structural implication of the kinetic analysis is that the cytoplasmic modulatory factors may interact with those elements of the Kv4 channel subunit that control inactivation gating at an internal site near the inner vestibule of the pore (Jerng et al., 1999). Preliminary parts of this study were previously reported in abstract form (Beck and Covarrubias, 1999, 2000).

## MATERIALS AND METHODS

### Molecular biology and cRNA microinjection

Wild-type mouse Kv4.1 is maintained in pBluescript II KS (Strategene, La Jolla, CA). Kv4.2 and Kv4.3 cDNAs (from rat) were kindly provided by Dr. J. Nerbonne (Washington University, St. Louis, MO), and are maintained in pRc/CMV (Invitrogen, Carlsbad, CA) and pBK-CMV (Strategene), respectively. Capped cRNA for expression in *Xenopus* oocytes was produced by in vitro transcription using the Message Machine Kit (Ambion, Austin, TX). Wild-type Kv4.1, Kv4.2, and Kv4.3 cRNAs were injected into defolliculated *Xenopus* oocytes (≤50 ng/cell) using a Nanoject microinjector (Drummond, Broomall, PA). Currents were recorded 1–7 days postinjection.

### Electrophysiology

Patch-clamp recording was conducted as described before (Chabala et al., 1993; Jerng et al., 1999) using an Axopatch 200A or 200B amplifier (Axon Instruments, Foster City, CA). Patch pipettes were constructed from Corning glass 7052 or 7056 pipettes (Warner Instrument Corp., Hamden, CT). For the recording of fast currents (e.g., tail relaxations) the pipettes were coated with Sylgard elastomer (Dow Corning Co. Midland, MI). Typically, for macropatch recording, the tip resistance of the recording pipettes in the bath solution (see below) was ≤1 MΩ. The pipette solution (external) contained (in mM): 96 NaCl, 2 KCl, 1 $MgCl_2$, 1.8 $CaCl_2$, 5 HEPES (pH 7.4, adjusted with NaOH). The bath solution (internal solution for IO patches) contained (in mM): 98 KCl, 0.5 $MgCl_2$, 1 EGTA, 10 HEPES (pH 7.2, adjusted with KOH). The passive leak current was subtracted off-line, assuming a linear leak current, or, alternatively, both the passive leak current and the capacitive transients were subtracted on-line using a P/4 procedure. The recordings were filtered at 0.5–8 kHz (−3 db, eight-pole Bessel filter; Frequency Devices, Haverhill, MA) and digitized at 2–40 kHz. All experiments were recorded at room temperature (23 ± 1°C).

### Data acquisition, analysis, and model simulations

A Pentium class computer interfaced to a 12-bit A/D converter (Digidata 1200 using Clampex 8.0; Axon Instruments) controlled the voltage-clamp protocols and data acquisition. Data analysis was conducted using Clampfit (pClamp 6.0 or Clampfit 8.0; Axon Instruments), and Origin (Microcal Software Inc., Northhampton, MA). Current relaxations and other time-dependent processes were described assuming a simple exponential function or the sum of exponential terms (Jerng and Covarrubias, 1997). Comparative kinetic analysis was restricted to data sets from patches that allowed paired recordings in the cell-attached (CA) and IO configurations. The development of inactivation of macroscopic Kv4 currents is complex (Jerng and Covarrubias, 1997). Thus, for an initial model-independent analysis of the kinetic changes induced by patch excision, the degree of inactivation is estimated by computing fractional inactivation at the time of the maximal difference (TMAX) in the development of inactivation between CA and IO currents (after normalizing the peaks). To optimize the measurement, TMAX is obtained after the development of inactivation changes no further (Fig. 1). Relative to the peak current, fractional inactivation of each trace is therefore computed as $I_{TMAX}/I_P$, where $I_{TMAX}$ is the current magnitude at TMAX and $I_P$ is the corresponding peak current. Fractional inactivation decreases as the currents accelerate. Thus, to represent enhanced inactivation more conveniently, we preferred to use the inverse relationship (degree of inactivation (DI) = $I_P/I_{TMAX}$; as this ratio increases, inactivation increases; Fig. 1). Unless indicated otherwise, all measurements are expressed as mean ± SEM. The Student's *t*-test or one-way ANOVA were used to evaluate the statistical significance of the observed differences (*P* values are given in the text, tables, and figure legends). Model simulations were conducted by determining the initial equilibrium probabilities of occupying a set of states and the characteristic differential equations of the model. For a particular pulse protocol and set of rate constants, this system of equations was solved numerically using SCoP 3.51w (Simulation Resources, Inc., Berrien Springs, MI). The simulations were evaluated by eye. A more quantitative simultaneous curve-fitting analysis was prevented by the kinetic variability (possibly due to heterogeneity) and the technical difficulty in obtaining complete data sets that examined at least five different voltage protocols from the same patch in both configurations.

## RESULTS

### Reversible modulation of the peak current and the development of inactivation in IO patches expressing Kv4.1 channels

If inactivation gating in Kv4.1 channels depends on the presence and integrity of cytoplasmic components that in-

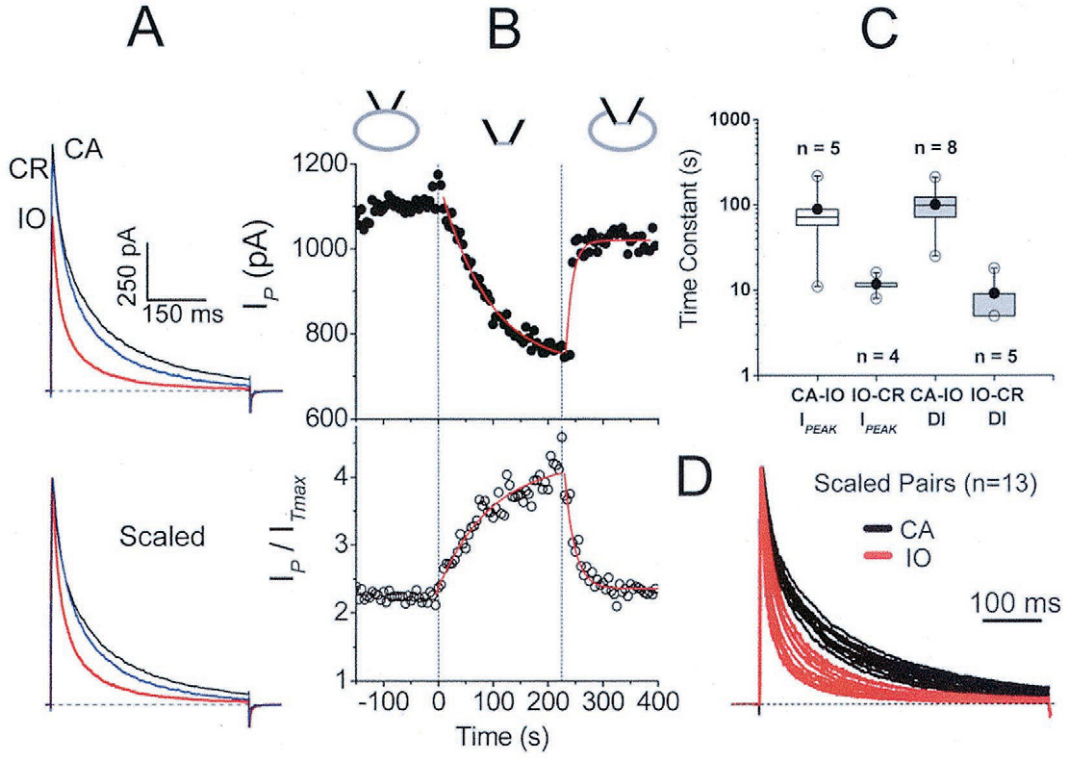


FIGURE 1 The effects of patch excision and patch cramming on macroscopic Kv4.1 currents expressed in *Xenopus* oocytes. (*A*) Macroscopic Kv4.1 currents evoked by a step depolarization from −100 to +50 mV. From the same patch, the currents are shown before (*CA*) and after (*IO*) patch excision, and after cramming the patch pipette into the oocyte (*CR*). Each trace represents the average of at least six consecutive responses. The currents are also shown scaled for a direct comparison of the development of inactivation (*bottom*). (*B*) The time courses of the changes in peak current ($I_P$, *filled symbols*) and the degree of inactivation (DI = $I_P/I_{TMAX}$, *open symbols*). Currents were evoked as explained above at intervals of 5 s (to insure recovery from inactivation). The *x* axis is the time during the experiment and each point represents a measurement from an individual response (0 marks the time of patch excision). $I_{TMAX}$ is the current amplitude corresponding to the maximum amplitude difference (at time TMAX) between the CA and IO currents at the end of the IO period (generally, steady state). For the example shown here, TMAX = 50 ms. Acceleration of the development of inactivation causes $I_{TMAX}$ to decrease significantly more than the decrease in $I_P$. Dotted lines flank the IO period. The solid lines represent the best-fit assuming exponential relaxations. The time constants were 88 s and 12 s for the changes in $I_P$, and 98 s and 18 s for the changes in DI. (*C*) Box plots comparing the time constants of the time-dependent changes in the peak current ($I_P$) and the DI. The time constants were extracted as explained above. The lower and upper borders of the box represent the 25th and 75th percentiles, respectively; and the whiskers correspond to the 10th and 90th percentiles. The line across the box represents the 50th percentile and the filled circle marks the mean value. The open circles represent the extreme values. Note that the time constants of the changes upon patch excision and cramming for $I_P$ and DI are similar ($p > 0.05$). The time constants of the development of the changes and the recovery are, however, significantly different ($p < 0.05$). (*D*) Macroscopic inactivation of Kv4.1 channels in 13 CA/IO pairs. Currents were evoked by a step-depolarization to +50 mV from a holding potential of −100 mV. To compare the development of inactivation, the peak of all traces was normalized.

teract with the channels, their function and importance can be inferred from kinetic differences between currents in CA and IO patches. In *Xenopus* oocytes, macropatch Kv4.1 outward currents at depolarized membrane potentials exhibit inactivation that develops over a period of several hundred milliseconds at positive membrane potentials (Jerng et al., 1999; Fig. 1). The development of inactivation is, however, accelerated upon patch excision and the peak current undergoes an apparent partial run down (Fig. 1 *A*). For a simple model-independent analysis, the DI in a given trace was computed as $I_P/I_{TMAX}$, where $I_P$ is the peak current and $I_{TMAX}$ is the corresponding current magnitude at the time of maximal difference between the decays of CA and IO currents (see Materials and Methods). This ratio is relatively constant in the CA configuration but increases in a time-dependent manner after patch excision ($I_{TMAX}$ decreases) as the development of inactivation accelerates and eventually reaches a steady-state level (i.e., an enhanced $I_P/I_{TMAX}$ corresponds to an enhanced degree of inactivation; Fig. 1 *B*). Concomitantly and following a similar time course, the peak current from IO patches decreases to a new level (Fig. 1 *B*; Table 1). These changes were reversible in a time-dependent manner upon cramming the patch into the oocyte (Fig. 1, *A* and *B*). The time dependencies of the changes in the peak current and current kinetics developed over periods lasting seconds to hundreds of seconds and are approximately exponential (Fig. 1, *B* and *C*). The time constants for the development of the changes are 112 ± 36 s ($n = 7$) and 112 ± 51 s ($n = 4$) for $I_P/I_{TMAX}$ and the apparent run-down, respectively. The kinetics of the rever-

**TABLE 1 The effects of patch excision on the peak current and the development of inactivation**

| Parameter | Kv4.1 | Kv4.3 | P† |
|---|---|---|---|
| $I_{PIO}/I_{PCA}$* | 0.72 ± 0.02<br>$n$ = 202 | 0.73 ± 0.06<br>$n$ = 9 | — |
| $I_P/I_{TMAX}$‡ | | | |
| CA | 1.97 ± 0.05 | 1.46 ± 0.04 | <0.01 |
| IO | 3.39 ± 0.11 | 2.26 ± 0.11 | |
| | $n$ = 143 | $n$ = 11 | |

*The ratio of the peak currents between inside-out (IO) and cell-attached (CA) patches.
†Statistical P-value (paired Student's $t$-test) evaluating the difference between the inactivation parameter ($I_P/I_{TMAX}$) from CA and IO patches.
‡Degree of inactivation as described in Materials and Methods. Because this parameter changes in a time-dependent manner upon patch excision (Fig. 1), the values reported here for IO patches are those obtained at steady-state.

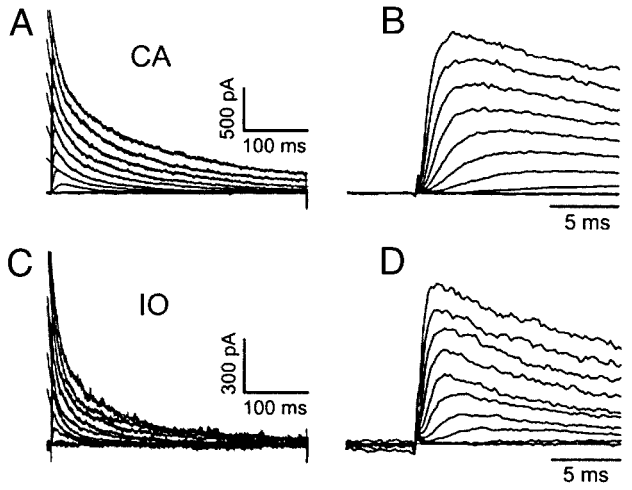


FIGURE 2 Kinetics of macroscopic Kv4.1 inactivation in CA and IO patches. (*A*) and (*C*) Macropatch outward currents evoked by 400-ms step depolarizations from a holding potential of −100 mV to various command potentials (−80 to +100 mV in 20-mV increments). The current traces and the best double-exponential fits are shown superimposed. (*B*) and (*D*) The corresponding first 15 ms of the currents shown in panels (*A*) and (*C*), respectively.

sal of the changes upon cramming was more difficult to measure because the currents were sampled every 5 s (to insure recovery from inactivation). Sometimes the reversal of the changes was almost complete within the first 5 s after cramming (Fig. 1 *B*). Nevertheless, upper-limit estimates of the time constants are similar for the reversal of changes in the degree of inactivation and the peak current (8.8 ± 1.4 s, $n$ = 4 and 13 ± 1.5 s, $n$ = 3 for $I_P/I_{TMAX}$ and IP, respectively). The similarities between the kinetics of the two empirical parameters suggest that the same mechanism may mediate all changes induced by patch excision. In some experiments, these changes were accelerated about 10-fold when the cytoplasmic face of the IO patch was perfused with the intracellular solution (data not shown). Thus, it seems that diffusible or labile cytoplasmic factors modulate Kv4.1 current kinetics in *Xenopus* oocytes. The kinetics and voltage dependence of Kv4.1 gating in CA and IO patches was examined in detail to gain insights into the mechanisms of inactivation and the kinetic basis of the changes induced by patch excision.

## Kv4.1 channels in IO patches exhibit modulation of macroscopic inactivation

Macroscopic inactivation of whole-oocyte Kv4.1 currents evoked by 1-s step depolarizations to positive voltages is generally well described, assuming the sum of at least three exponential terms (in a manner that is independent of current magnitude; Jerng and Covarrubias, 1997; Jerng et al., 1999). In CA macropatches, the kinetics of Kv4.1 macroscopic inactivation is similar to that seen in whole-oocytes, albeit exhibiting greater variability (Fig. 1 *D*). In many cases, the sum of two exponential terms was sufficient to describe macropatch currents that appeared to inactivate more rapidly. By contrast, inactivation of macroscopic currents from IO patches is always faster than that of the corresponding CA currents, and is well described, assuming the sum of two exponential terms (Fig. 1 *D*). For a simpler, more quantitative comparison of inactivation kinetics between currents in CA and IO patches, a biexponential function was used to empirically describe the currents evoked by 400-ms step depolarizations between −20 and +110 mV (Figs. 2 and 3). This pulse duration was sufficient to inactivate >80% of the CA and >95% of the IO currents examined in Fig. 2. Such an analysis allowed us to test whether faster IO currents exhibited reduced time constants of inactivation or shifts in the relative weights of the two apparent phases of inactivation. Although the fast phase might be predominantly associated with open-state inactivation, the slow one is significantly influenced by closed-state inactivation in Kv4.1 channels (Jerng et al., 1999).

The fast time constants of macroscopic inactivation (15–25 ms) decrease moderately with depolarization and, at modestly depolarized voltages, appear smaller in IO patches (Fig. 3 *B*). The slow time constants of CA currents, in contrast, increase with depolarization between +10 and +110 mV (120 ± 17 and 186 ± 19 ms, respectively; $p < 0.05$; Fig. 3 *B*). Such a behavior has been previously observed in Kv4 channels (Chabala et al., 1993; Jerng and Covarrubias, 1997; Hoffman et al., 1997) and is reminiscent of preferential closed-state inactivation (Klemic et al., 1998). Importantly, IO currents exhibit significantly reduced slow time constants of inactivation ($p < 0.01$), which also increase with depolarization (66 ± 6 to 112 ± 12 ms, between +10 and +110 mV, respectively; $p < 0.01$; Fig. 3 *B*); and the voltage-independent amplitude ratio ($A_F/A_S$) is significantly increased (i.e., the fast phase becomes dominant in IO patches; Fig. 3 *C*; $p < 0.01$). Probably as a result

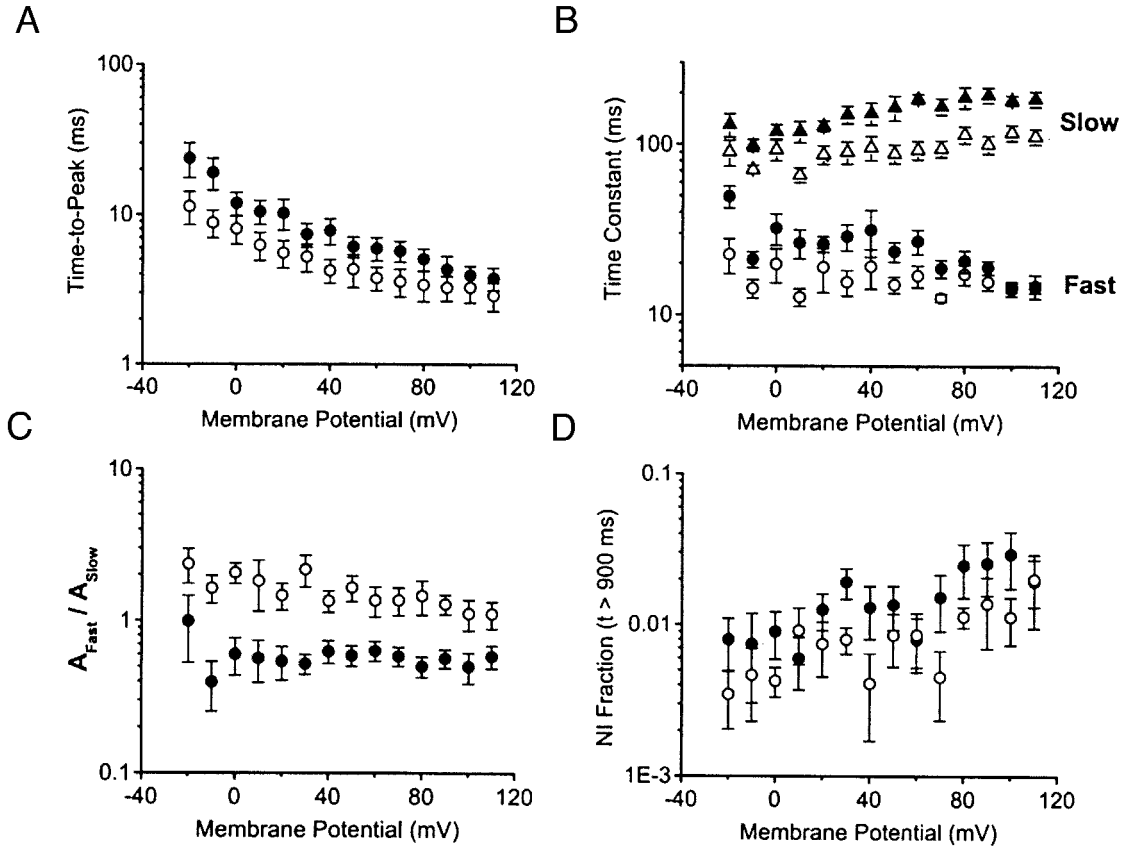


FIGURE 3 Description of macroscopic Kv4.1 currents using empirical parameters. (*A*) Voltage dependence of the time-to-peak. (*B*) Voltage dependence of the fast (*circles*) and slow (*triangles*) time constants of macroscopic inactivation. The difference between the CA and IO slow time constants is statistically significant ($p < 0.01$) throughout the examined voltage range. (*C*) Voltage-dependence of the amplitude ratio ($A_{Fast}/A_{Slow}$) extracted from the biexponential analysis of macroscopic inactivation. The difference between the CA and IO amplitude ratios is statistically significant ($p < 0.01$) throughout the examined voltage range. (*D*) Voltage-dependence of the noninactivating fraction derived from multiexponential fits (2–3 terms) to the decay of macroscopic currents (pulse duration $\geq$ 500 ms). Thus, NI fraction = $A_{NI}/(A_{Fast} + A_{Slow} + A_{NI})$, where $A_{NI}$ is the amplitude of the noninactivating component of the current) as determined from the constant term of the multiexponential fits; $A_{Fast}$ and $A_{Slow}$ are corresponding amplitudes of the fast and slow terms, respectively. The slowest time constant of the triple exponential fits was ~250–300 ms and was weakly voltage dependent; Jerng and Covarrubias; 1997. The difference between the NI fractional values from CA and IO patches is not statistically significant ($p > 0.05$) throughout the examined voltage range. In all panels, the symbols represent the mean values of 4–8 paired CA/IO patches.

of accelerated inactivation, the time-to-peak of the IO currents appears slightly shortened (Fig. 3 *A*). With long depolarizing pulses ($\geq$1 s), inactivation of Kv4.1 channels is almost complete at all relevant voltages. Accordingly, the noninactivating fraction of the fitted current decay is very small ($<$0.05) and nearly voltage independent. This parameter remains unchanged in both patch configurations (Fig. 3 *D*). Thus, accelerated macroscopic inactivation of Kv4.1 currents in IO patches at positive voltages is mainly the result of a faster slow phase and the enhanced relative amplitude of the fast phase.

## Closed-state inactivation in Kv4.1 channels is more favorable in IO patches

An important pathway of inactivation in Kv4.1 channels originates from closed states (Jerng et al., 1999). Because the channel opening does not appear to be strongly favored (even at the most positive membrane potentials) in these channels, they might inactivate significantly from the preopen inactivation permissive closed state. Thus, it is conceivable that faster closed-state inactivation underlies the acceleration of macroscopic inactivation at positive voltages (Figs. 2 and 3). To test this hypothesis, we isolated closed-state inactivation by examining the development of inactivation at negative voltages (−90, −70, −60 and −50 mV) in paired CA and IO patches expressing Kv4.1 currents (Fig. 4). In these experiments, a pulse to +50 mV tests the available current from a hyperpolarized holding voltage (−100 mV; control) and from progressively prolonged prepulses (in discrete logarithmic intervals between 50 and 6000 ms) (Fig. 4, *A* and *B*). The prepulses examined here open a negligible fraction of the available channels (see Fig. 9). Thus, the inactivation induced by this protocol is mostly

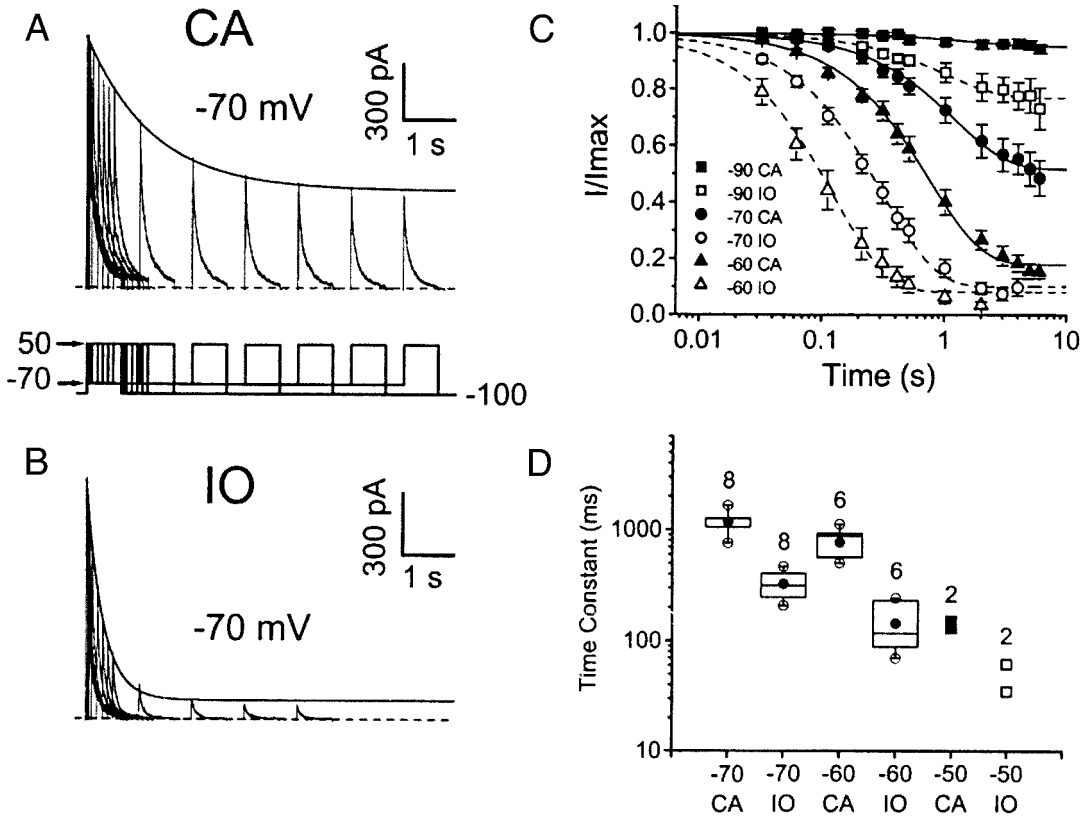


FIGURE 4 Kinetics of Kv4.1 inactivation at negative membrane potentials (closed-state inactivation) in CA and IO patches. (A) and (*B*) Consecutive current traces evoked by a step depolarization to +50 mV. Except for the first trace (far-left), which was evoked from a holding potential of −100 mV (control), subsequent currents were evoked from an increasingly prolonged prepulse at −70 mV. The pulse protocol is shown below the set of CA traces. (*C*) Time courses of closed-state inactivation at various membrane potentials. The data points are normalized peak currents evoked as explained above. The normalized values resulted from dividing the peak currents (*I*) evoked from the indicated voltages by the peak control current (*Imax*). Each symbol represents the mean value of 6–8-paired experiments. The solid and dashed lines are the best-fit exponential curves that describe inactivation in CA and IO patches, respectively. (*D*) Box plots (see Fig. 1 legend) comparing the voltage-dependence of the time constants of closed state inactivation. The number of experiments is shown above the box. At −50 mV, only two paired measurements were taken.

originating from closed states in the activation pathway. As the prepulse duration increases, channels inactivate and the peak current decreases gradually and eventually reaches a steady-state level (Fig. 4, *A–C*). The development of inactivation at all tested prepulses was (relative to the kinetics in CA patches) clearly accelerated in IO patches and well described, assuming an exponential decay (Fig. 4, *A–C*). For instance, in CA and IO patches, the time constants of inactivation at −70 mV were 1200 ± 100 and 330 ± 30 ms ($n = 8$; $p < 0.01$), respectively (Table 2). The small amplitude of the current change at −90 mV in these experiments prevented a reliable measurement of the time constant. Better measurements at −90 mV were, however, obtained from the time course of recovery from inactivation (see below). Inactivation at steady state is also more profound in IO patches (at the four tested prepulses). Consistently reduced time constants of inactivation from IO patches in these experiments clearly suggest that closed-state inactivation in Kv4.1 channels is more favorable in the IO patch configuration (Fig. 4 *D*). Consequently, the voltage dependence of steady-state (prepulse) inactivation of channels in IO patches is shifted toward more negative voltages (relative to CA patches, as demonstrated later; Fig. 6; Table 2).

Such a shift does not bear a contribution of altered recovery from inactivation because its time course was not significantly altered by patch excision. Recovery from inactivation was examined at −120, −100, −90 and −80 mV in paired CA and IO patches expressing Kv4.1 macroscopic currents (Fig. 5). In both configurations, the time courses of recovery from inactivation are relatively fast (reaching steady-state in <4 s), approximately exponential and voltage dependent. However, it is clearly apparent that, especially at −80 mV, the level of steady-state inactivation was more profound in IO patches. This observation is also consistent with a hyperpolarizing shift in the midpoint of steady-state inactivation (Fig. 6).

This conclusion is firmly confirmed by examining the voltage dependence of steady-state (prepulse) inactivation between −110 and −30 mV for paired CA/IO experiments

**TABLE 2 Parameters of inactivation gating at negative membrane potentials**

| | Kv4.1 | | Kv4.3 | |
|---|---|---|---|---|
| | CA | IO | CA | IO |
| $\tau$-inactivation* at −70 mV (s) | 1.2 ± 0.1<br>$n = 8$ | 0.3 ± 0.033<br>$n = 8$<br>$P < 0.01^\dagger$ | 5.2 ± 1.2<br>$n = 5$ | 1.5 ± 0.5<br>$n = 5$<br>$P < 0.5^\dagger$ |
| $V_{1/2}^\ddagger$ (mV) | −72.3 ± 1.9<br>$n = 6$ | −82.5 ± 1.6<br>$n = 6$<br>$P < 0.01^\dagger$ | −70.3 ± 2.6<br>$n = 10$ | −81.7 ± 1.8<br>$n = 10$<br>$P < 0.01^\dagger$ |
| $k^\S$ (mV) | 4.7 ± 0.17<br>$n = 6$ | 5.0 ± 0.1<br>$n = 6$<br>$P > 0.05^\dagger$ | 3.7 ± 0.2<br>$n = 10$ | 4.1 ± 0.2<br>$n = 10$<br>$P > 0.05^\dagger$ |

*Time constant of inactivation determined as described in Fig. 4 legend.
†Paired Student's *t*-test.
‡Midpoint voltage determined from fitting a first-order Boltzmann distribution to the voltage dependence of steady-state (prepulse) inactivation (Fig. 6).
§Corresponding slope factor.

(Fig. 6). As expected from the kinetic analysis (Figs. 4 and 5), the prepulse inactivation curves in six separate experiments from IO patches are negatively shifted relative to the corresponding CA patch (but maintain similar voltage sensitivities). These curves were well described, assuming first-order Boltzmann functions (three out of six curves shown in Fig. 6; Table 2). From these results, it appears conceivable that the reduced peak current and accelerated inactivation of

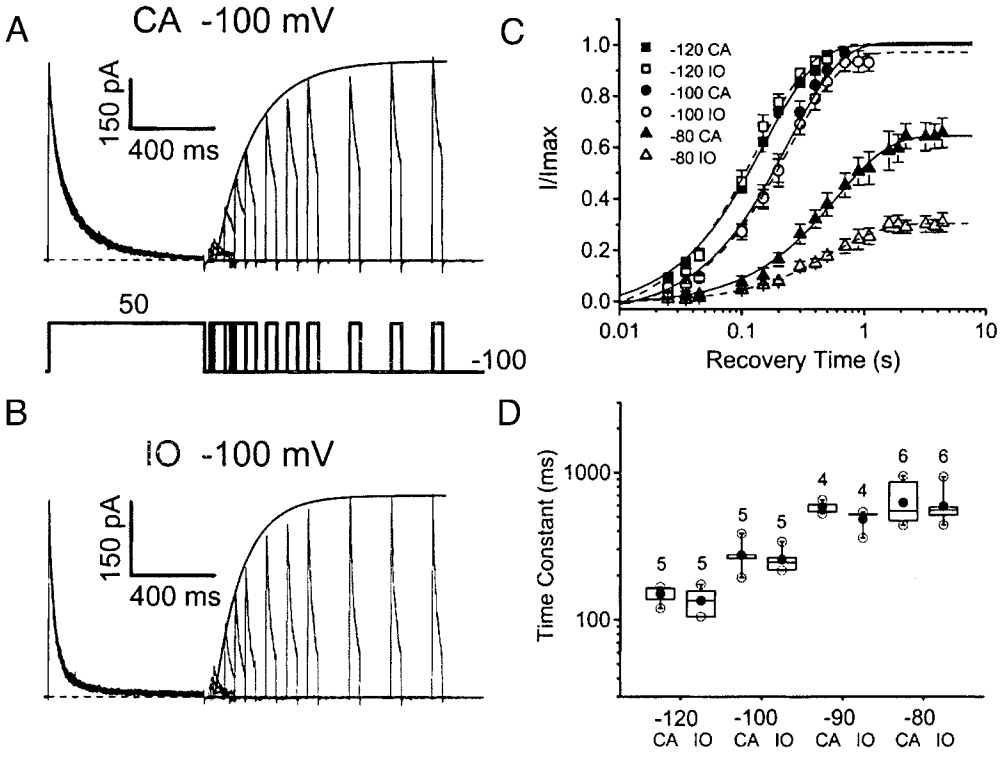


FIGURE 5 Kinetics of recovery from inactivation of Kv4.1 channels in CA and IO patches. (*A*) and (*B*) Currents evoked by a double pulse protocol to investigate the kinetics of recovery from inactivation. The first pulse (from −100 to +50 mV) allows activation and inactivation of the evoked current, and the second, shorter pulse (+50 mV) tests the amount of current recovered after an increasingly prolonged interpulse interval (at −100 mV). The pulse protocol is shown below the CA traces. (*C*) The time course of recovery from inactivation at various interpulse voltages. The data points are normalized peak currents evoked as explained above. The normalized value is the result of dividing the test peak currents (*I*) by the corresponding control peak current (*Imax*). Each symbol represents the mean value of 4–5 paired experiments. The solid and dashed lines are the best-fit exponential curves that describe recovery from inactivation in CA and IO patches, respectively. At −80 mV, the recovery is incomplete because, at that voltage, a significant fraction of the channels remains inactivated at steady state (~35% and ~70% in CA and IO, respectively). (*D*) Box plots (see Fig. 1, legend) comparing the voltage-dependence of the time constants of closed state inactivation. The number of experiments is shown above the box.

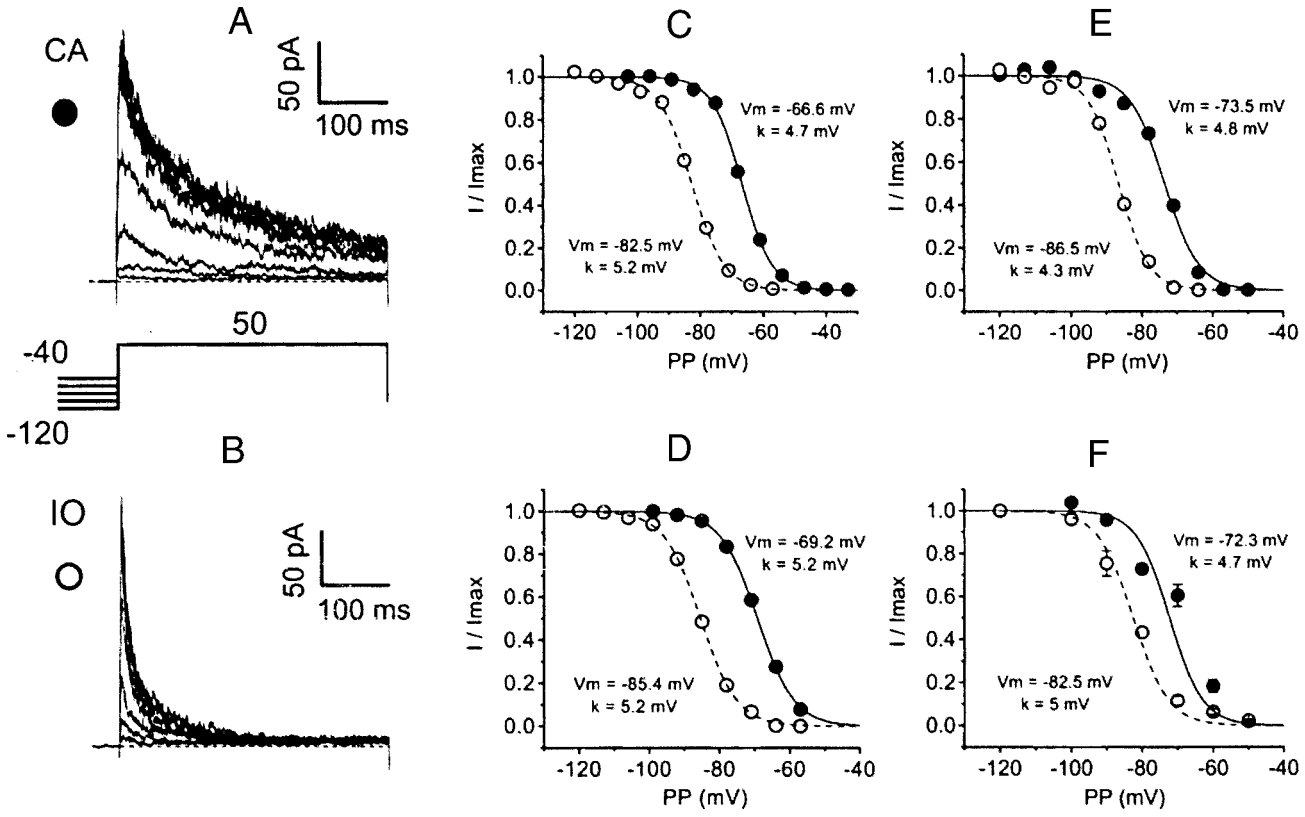


FIGURE 6 Steady-state prepulse inactivation of Kv4.1 channels in CA and IO patches. (*A*) and (*B*) Outward currents evoked by a step depolarization to +50 mV from various prepulse holding potentials ranging between −120 and −40 mV at 10-mV intervals. To ensure steady state, the length of the prepulse was 10 s (see Fig. 3; Table 1). The pulse protocol is shown below panel (*A*). (*C*, *D*, *E*, F) Relation between the prepulse potential and the normalized peak current (*I*/*Imax*). The solid and dashed lines are the best-fit first-order Boltzmann distributions. The best-fit parameters ($V_m$ and slope factor) are shown on the left and right sides of the corresponding curves. Panels (*C*), (*D*), and (*E*) show the data from three independently paired CA-IO patches. The data points in panel (*F*) are the pooled estimates of the steady-state amplitudes obtained from the development of closed-state inactivation and recovery from inactivation (Figs. 4 and 5). The averaged best-fit Boltzmann parameters from 6-paired experiments (CA-IO pairs; Table 2) were used to generate the solid and dashed lines in panel (*F*).

Kv4.1 channels in IO patches at both negative and positive voltages is the result of more favorable closed-state inactivation (see Discussion).

## Deactivation of Kv4.1 channels is modestly accelerated in IO patches

The dominant slow pathway of inactivation in Kv4.1 channels appears to be coupled to channel closing (see above; Jerng et al., 1999). Thus, if the closing rate changes, the occupancy of the preopen inactivation-permissive closed state is affected, and, consequently, the observed rate of slow macroscopic inactivation changes too. To investigate the possible influence of channel closing on the development of macroscopic inactivation, tail current deactivation was examined at various membrane potentials (−140 to −50 mV) in paired CA/IO patches (Fig. 7). Because channel closing in Kv4.1 channels appears to be rate limiting, fast tail current relaxations at hyperpolarized voltages (−140 to −100 mV) mostly reflect the weakly voltage-dependent O→C transition (Jerng et al., 1999). Another frequently resolved kinetic component of the tail current at hyperpolarized voltages might correspond to the reopening of a small fraction of channels that had already inactivated from the open state when the current reached its peak (I→O; Jerng et al., 1999). Thus, in most instances, the tail currents from CA and IO patches were well described, assuming the sum of two exponential terms (with a dominant fast component at hyperpolarized voltages; Fig. 7). At more depolarized voltages, the processes underlying the tail current relaxations are more confounded because, in addition to channel closing, they bear a contribution of voltage-dependent transitions in the activation pathway. Although the time constants of tail current deactivation from IO patches were clearly smaller in some paired CA/IO experiments (Fig. 7, *A–B*), this difference could not be conclusively demonstrated after examining several batches of oocytes (Fig. 7, *C–D*; even though the currents tested in these

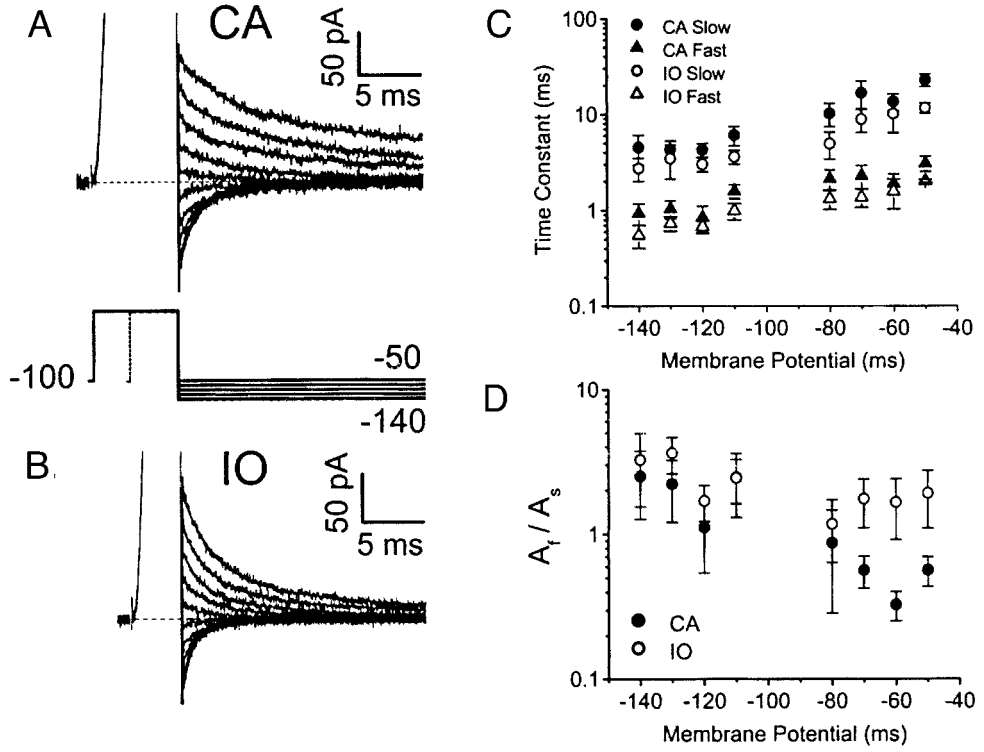


FIGURE 7 Deactivation of Kv4.1 currents in CA and IO patches. (*A*) and (*B*) Tail currents evoked by the pulse protocol shown below the traces in panel (*A*). The outward current evoked by the pulse to +50 mV has been clipped to emphasize visualization of the inward tail current. Note that, because the IO currents tend to reach their peak earlier, the pulse to +50 mV is shorter (*dashed line* in the waveform diagram). Smooth lines superimposed on the current traces are the best double exponential fits. (*C*) Voltage-dependence of the fast and slow time constants extracted from the double exponential fits to the tail current relaxations. Differences between CA and IO values were not significant ($p > 0.05$; except at −50 mV, $p < 0.05$). (*D*) Voltage dependence of the amplitude ratios ($A_f/A_s$) extracted from double exponential fits to the tail current relaxations. The symbols in all panels represent the mean values of 3–4 experiments.

experiments exhibited significantly accelerated inactivation at positive voltages in IO patches). At −140 mV for instance, $\tau_{FAST} = 0.9 \pm 0.2$ ms and $0.6 \pm 0.1$ ms from CA and IO patches ($n = 4$; $p > 0.05$), respectively. The slow time constant at −50 mV probably exhibits the most significant change ($\tau_{SLOW} = 22.6 \pm 3.5$ ms and $11.6 \pm 1.4$ ms from CA and IO patches ($n = 3$; $p < 0.05$), respectively) and the relative amplitudes of the fast component at depolarized voltages (−70 to −50 mV; Fig. 7 *D*) also appear increased. To further improve resolution, attempts were made to demonstrate reduced time constants of deactivation in IO patches in symmetrical ionic conditions (98 mM KCl). These experiments exhibited a trend similar to that described above but also failed to show a statistically significant acceleration of deactivation (data not shown; M. Shahidullah and M. Covarrubias, manuscript in preparation). These results suggest that accelerated channel closing might also contribute to faster macroscopic inactivation in IO patches, but, given the experimental variability, such a role is more difficult to demonstrate in our experimental conditions. It must be noted, however, that accelerated channel closing can further contribute to accelerated closed-state inactivation because that change favors the occupancy of the preopen inactivation-permissive closed state (see Discussion).

## The peak G–V relation does not appear significantly altered in IO patches

Because the prepulse inactivation curves from IO patches appeared leftward shifted, it is conceivable that, in addition to more favorable closed-state inactivation (see above), voltage-dependent activation could have also been shifted by patch excision. To test this hypothesis, we examined the peak conductance–voltage relations (Gp–V curves) recorded from paired CA and IO patches (Fig. 8). Although the Gp–V curve of Kv4 channels does not reflect the true activation curve of these channels (due to pronounced inactivation), it provides a relative measurement of changes that might influence voltage-dependent activation. Independently of patch configuration, the Gp clearly begins to rise at ~−55 mV, increases more steeply between −40 and 0 mV, and levels off gradually between +10 and +120 mV.

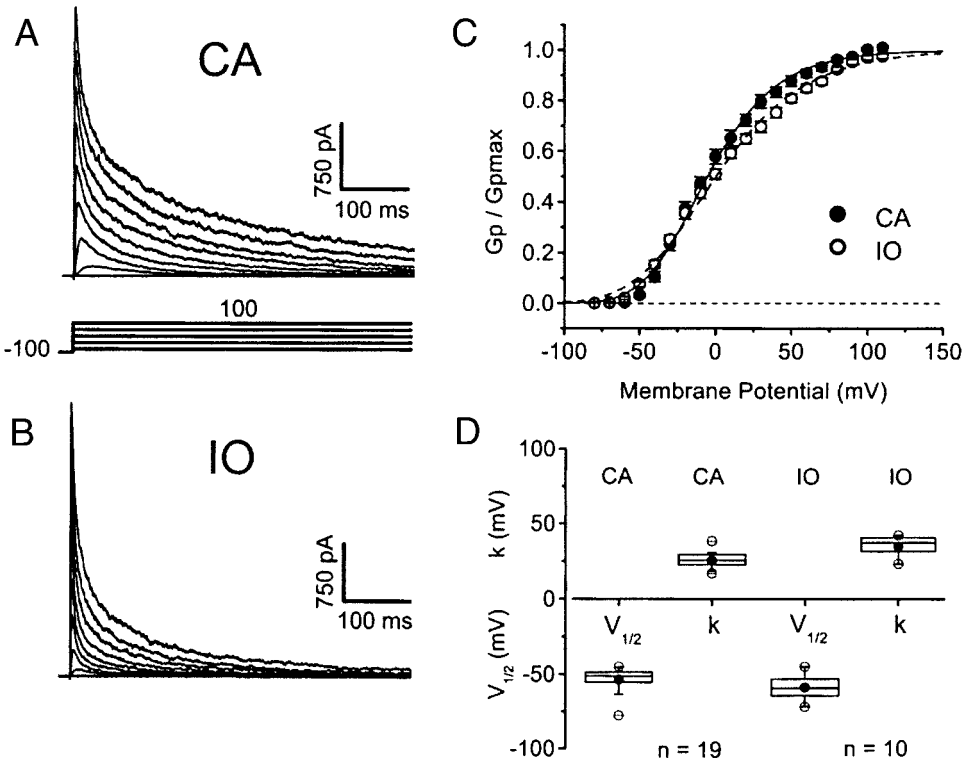


FIGURE 8 The peak conductance–voltage relation of Kv4.1 channels in CA and IO patches. (*A*) and (*B*) Outward currents evoked by step depolarizations from a holding potential of −100 mV to test potentials ranging from −80 to +100 mV in 20-mV increments. (*C*) The corresponding peak conductance–voltage relation (Gp–Vt) derived from currents evoked by the pulse protocol described above ($n$ = 11 paired CA/IO recordings). The peak chord conductance (Gp) was calculated from the following relation: Gp = $I$p/(Vt − Vr), where $I$p is the peak current, Vt is the test potential and Vr is the reversal potential of the current (−93 to −95 mV, as determined from the instantaneous current–voltage relation derived from the corresponding tail current experiments). The instantaneous current–voltage relations are linear over the range of voltages where the channels activate (not shown). The solid lines represent the best-fit fourth-order Boltzmann functions (Smith-Maxwell et al., 1998). The parameters of these fits were: $V_{1/2}$ = −53 and −61 mV for CA and IO, respectively; and $k$ = 29 and 37 mV/e-fold change, for CA and IO, respectively ($V_{1/2}$ is the midpoint voltage for the activation of one subunit, and $k$ is the corresponding slope factor). The data are shown normalized to the maximum estimated peak conductance (Gpmax). (*D*) Box plots summarizing the parameters derived from fourth-order Boltzmann fits (total number of examined curves is indicated at the bottom of the plot; paired and unpaired recordings).

The Gp–V curves were empirically described, assuming a fourth-order Boltzmann function (Fig. 8, legend). The shape of the Gp–V curves was somewhat variable, but there were no significant differences between the apparent "threshold" of activation for currents from CA and IO patches (−60 to −50 mV). Such a variable behavior mainly influenced the slope factor (the steepness of the curve), which ranged between 18 and 40 mV/e-fold with larger values in patches that exhibited significantly accelerated inactivation (Fig. 8 *D*). The Gp–V parameters reported here for Kv4.1 in CA patches are similar to those previously reported in our laboratory (Jerng and Covarrubias, 1997; Jerng et al., 1999). This analysis therefore shows that Kv4.1 currents in CA and IO patches begin to activate at similar voltages and that the accelerated kinetics of inactivation in IO patches might mainly decrease the observed steepness of the Gp–V curve. Thus it seems unlikely that significantly altered voltage-dependent activation additionally contributes to the hyperpolarizing shift of the prepulse inactivation curve in IO patches. The possible influence that faster deactivation might have on the true activation curve is confounded by excessive inactivation influencing the shape and amplitude of the Gp–V curve.

## All mammalian members of the Kv4 subfamily exhibit modulation of closed-state inactivation

Is the selective modulation of closed-state inactivation in IO patches unique to Kv4.1 channels, or does it represent a more fundamental property that is also characteristic of other known mammalian members of the Kv4 subfamily (Kv4.2 and Kv4.3)? This is a relevant question because all cardiac and neuronal Kv4 channels are highly conserved and mediate A-type $K^+$ currents, and we have previously hypothesized that these channels operate similarly and share the same mechanisms of inactivation (Jerng et al., 1999). Although, in CA patches, Kv4.3 macroscopic currents at

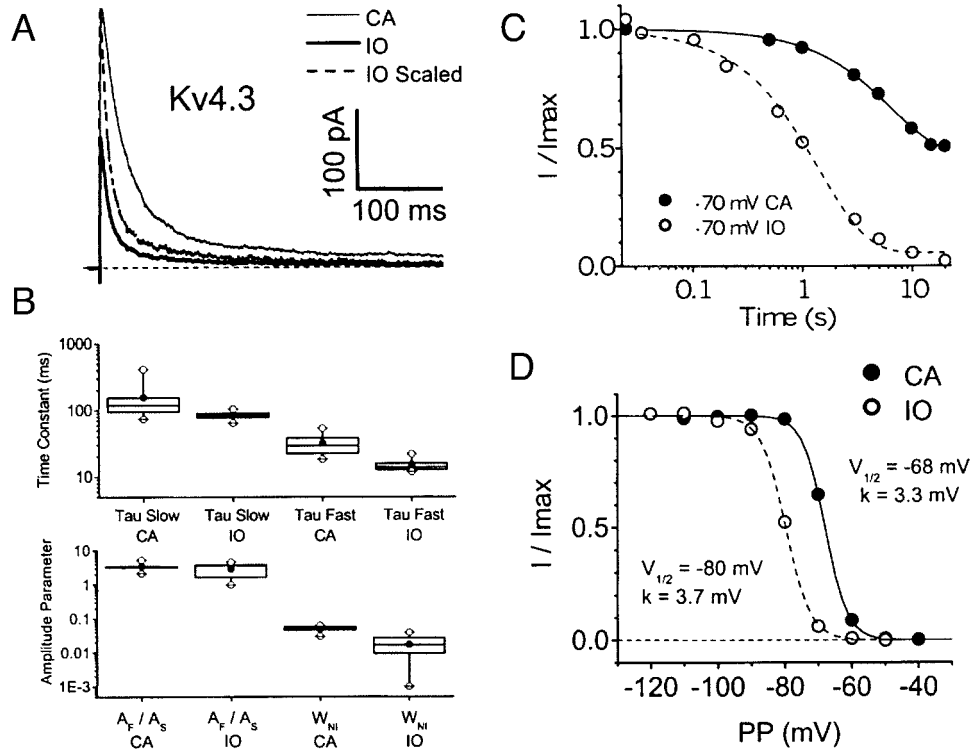


FIGURE 9 The effects of patch excision on the development of inactivation in Kv4.3 channels. (*A*) Outward currents evoked by a depolarization to +50 mV from a holding potential of −100 mV. Note that the current from the IO patch exhibits a reduced peak and an accelerated development of inactivation. (*B*) Box plots summarizing the best fit parameters extracted from fitting a double exponential function (plus a constant term) to the development of inactivation (see Fig. 2). $W_{NI}$ is the fraction of the current that does not inactivate as estimated from the constant term of the double exponential fits. (*C*) The development of closed-state inactivation in CA and IO patches at −70 mV. For more details on the pulse protocol see Fig. 4. The solid and dashed lines are the best-fit exponentials. The time constants obtained from these fits were: 6.5 and 1.4 s for CA and IO currents, respectively. (*D*) Prepulse inactivation in CA and IO patches. For more details on the pulse protocol see Fig. 6. The prepulse duration was 20 s because closed-state inactivation in Kv4.3 channels develops more slowly (Table 1). The solid and dashed lines are the best-fit first-order Boltzmann functions. The parameters of these fits (midpoint voltage, $V_{1/2}$ and slope factor, k) are shown in the plot.

positive voltages decay faster than those mediated by Kv4.1 channels, upon patch excision, Kv4.3 currents were also accelerated (Fig. 9). Importantly, closed-state inactivation is clearly faster, and such acceleration underlies the observed hyperpolarizing shift (~10–15 mV) in the prepulse inactivation curve (Figs. 4, 6, and 9; Table 2). Kv4.2 currents also exhibited faster macroscopic inactivation in IO oocyte patches (M. Shahidullah and M. Covarrubias, unpublished), but low Kv4.2 expression in oocyte macropatches precluded a more detailed analysis of these currents. Interestingly, however, the midpoint of steady-state prepulse inactivation (prepulse duration ≥10 s) varies significantly over a range of ~20 mV (from −63 to −83 mV) in both *Xenopus* oocytes (whole-oocyte currents) and mammalian cells (whole-cell currents expressed in COS-7 and TSA-201 cells) (R. Hernandez-Pineda, M. T. Pacheco-Cano and M. Covarrubias, unpublished). Such variable results have been previously documented in various cell types expressing Kv4.2 (Petersen and Nerbonne, 1999). These observations suggest that the properties of inactivation gating in Kv4.2 channels are consistent with those found in Kv4.1 and Kv4.3 channels.

The overall kinetic changes imposed by patch excision on Kv4.1 and Kv4.3 currents were very similar (Table 2). However, a more quantitative comparison (biexponential fits) of the development of inactivation of Kv4.1 and Kv4.3 outward currents at positive voltages revealed interesting differences. In Kv4.3 channels, mainly the fast time constant of macroscopic inactivation at +50 mV was significantly reduced in IO patches (Fig. 9, *A–B*). In contrast, mainly the slow component of Kv4.1 current decay at positive voltages was significantly altered in IO patches (Fig. 3). These differences do not necessarily represent qualitatively distinct mechanisms of inactivation among different members of the Kv4 subfamily. A greater contribution of closed-state inactivation to the fast component of the development of inactivation in Kv4.3 channels might explain the apparent discrepancy (see Discussion). Thus, the data suggest that all mammalian Kv4 channels undergo significant selective modulation of closed-state inactivation

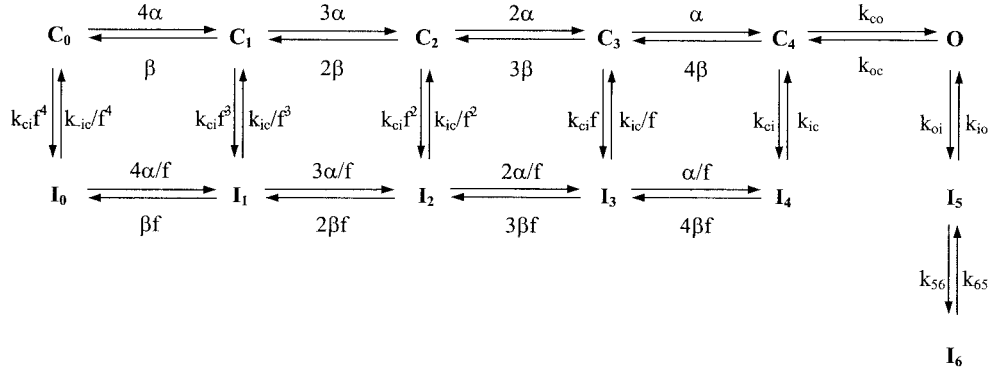


SCHEME 1

probably mediated by a similar mechanism involving critical cytoplasmic factors.

## DISCUSSION

We have investigated the biophysical properties of macroscopic currents mediated by Kv4 channels (Kv4.1 and Kv4.3) in CA and IO patches from *Xenopus* oocytes. The main goal of this study was to gain insights into the mechanisms of inactivation gating of these channels. In contrast to the mechanisms of Shaker $K^+$ channels, those of Kv4 channels are not well understood. Upon patch excision, initial observations demonstrated decreased peak current amplitudes and an accelerated development of macroscopic inactivation (Beck and Covarrubias, 1999, 2000). This study revealed that these changes are consistent with more favorable closed-state inactivation, which could influence the development of macroscopic inactivation at both negative and positive voltages (see below). The observed changes were readily reversible upon patch cramming. Therefore, the underlying molecular mechanism involves cytoplasmic factors that modulate closed-state inactivation of Kv4 channels at an internal site. Although most of our experiments were conducted with Kv4.1, we have also obtained evidence demonstrating that Kv4.2 and Kv4.3 undergo similar modulation. To understand the results more quantitatively, we have developed an allosteric state diagram as a working hypothesis that explains gating of Kv4 channels and modulation of inactivation. Particular attention was placed on explaining the following behaviors and changes upon patch excision: 1) a moderate U-shape of the voltage dependence of the time constants of inactivation over the voltage range where the channels exhibit activation (both in CA and IO); 2) accelerated macroscopic inactivation at positive voltages (with a dominant fast component and an accelerated slow component); 3) a reduction of the peak current (70–80% of control); 4) a slightly shallower Gp–V curve with no change in the apparent activation threshold; 5) an accelerated time course of closed-state inactivation at negative voltages; 6) minimal changes in the recovery from inactivation at hyperpolarized voltages; 7) variable, but possibly faster tail current relaxations; and 8) a leftward shift of the prepulse inactivation curve (~10 mV).

### An allosteric mechanism explains inactivation gating in Kv4 channels and the kinetic changes induced by patch excision

If the C↔O equilibrium in Kv4 channels is weakly voltage dependent and not strongly forward biased, inactivation from the preopen closed state may contribute significantly to inactivation at all relevant voltages (Jerng et al., 1999). Effectively, even at voltages that maximally activate these channels (>+100 mV), closing must occur before they undergo final and almost complete inactivation (i.e., inactivation is coupled to channel closing). To test whether this hypothesis can explain gating of Kv4.1 channels over a wide voltage range (−140 to +110 mV) and the preferential modulation of closed-state inactivation in IO patches, we simulated the kinetics and voltage dependence of the currents assuming a time-homogeneous allosteric kinetic model involving five closed states, one open state, and seven inactivated states (Scheme 1; Materials and Methods). Here, closed and inactivated states are allosterically coupled (e.g., Campbell et al., 1993; Kuo and Bean, 1994; Ayer and Sigworth, 1997; Olcese et al., 1997; Klemic et al., 1998) and channels can also inactivate directly from the open state, but open-state inactivation is unstable (forward rate = backward rate). Sequential transitions between closed states in the activation pathway are strongly voltage-dependent ($z \sim 10\ e_0$), but the opening equilibrium is weakly voltage-dependent ($z = 0.2\ e_0$) and the C↔I and O↔I equilibriums are assumed voltage-independent. It is also assumed that the molecular bases of open-state and closed-state inactivation are distinct (Jerng and Covarrubias, 1997; Jerng et al., 1999), and that open-state inactivation may involve two sequential conformational changes (Solc and Aldrich, 1991). A subset of this model, which mainly examined transitions near the open state, accounted

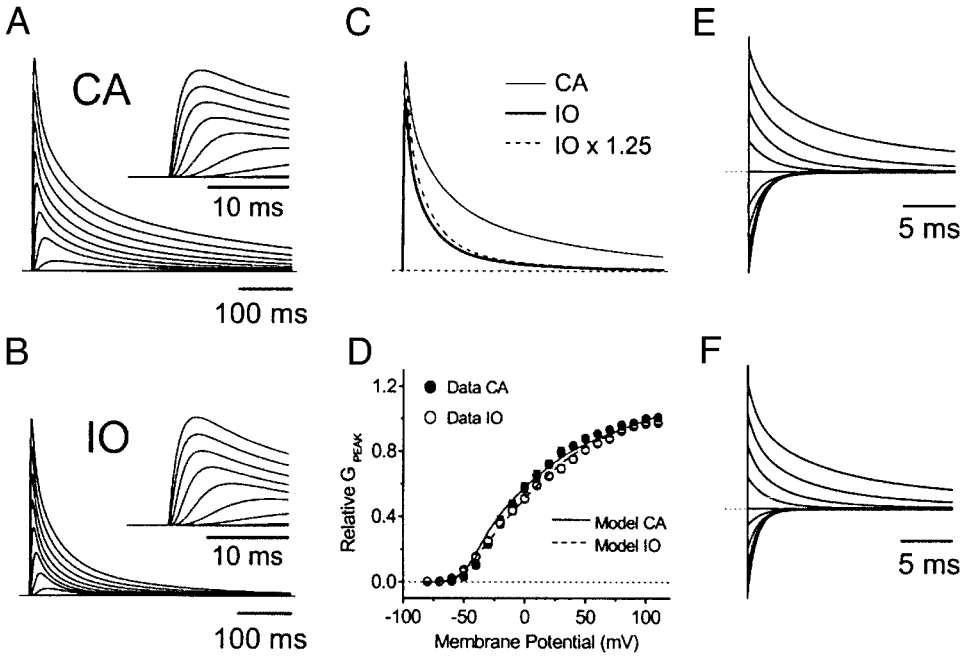


FIGURE 10 Simulations generated from Scheme 1 (activation and deactivation). All simulations shown here attempt to model the average behavior of Kv4.1 currents expressed in *Xenopus* oocyte macropatches (CA and IO). The parameters used for these simulations are shown in Table 3. (*A*) and (*B*) Simulated outward currents evoked by the voltage protocol described in Fig. 8. (*C*) Comparison of the currents evoked from −100 to +50 mV. TMAX is 73 ms and the DI values (degree of inactivation) extracted from the simulated currents are 2.4 and 4.8 for CA and IO, respectively (Fig. 1, *legend*). (*D*) Observed (*symbols*) and simulated (*lines*) Gp–Vt relations (Fig. 8, *legend*; the simulations assume Vr = −90 mV). (*E*) and (*F*) Simulated tail currents evoked by the voltage protocol described in Fig. 7. By fitting a polynomial function to observed instantaneous current-voltage relations, the simulated tail currents were accordingly corrected to account for open channel rectification near the reversal potential.

for the complex inactivation kinetics of Kv4.1 currents at positive voltages and the interaction between channel closing and inactivation gating (Jerng et al., 1999). In the expanded new model (Scheme 1), channels mainly occupy $I_4$ at the end of a long depolarization, and, from that state, they quickly recover upon hyperpolarization. Rapid recovery from inactivation is characteristic of recombinant Kv4 channels expressed in heterologous systems and native Kv4-like channels. Thus, the presence of a previously assumed deep inactivated state originating from $I_4$ (Jerng et al., 1999) is not consistent with rapid recovery from inactivation and has been eliminated from the new model.

Scheme 1 generated simulated currents with the kinetic and voltage dependent properties that closely mimic the behavior of Kv4.1 channels in CA and IO patches (Figs. 10 and 11; Table 3). All changes induced by patch-excision can be economically explained by preferentially enhancing the rate of closed-state inactivation ($k_{ci(IO)} = 2.5k_{ci(CA)}$; Table 3). Importantly, the peak G–V relations derived from the modeled currents are only slightly affected and superimpose closely with the observations (Fig. 10 *D*). This analysis demonstrates that important changes in the development of inactivation could occur in the absence of a significantly altered peak G–V relation (which mainly appears moderately shallower in IO patches). The voltage dependence of the inactivation time constants empirically extracted from the simulated currents is also in excellent agreement with the data (Fig. 11 *C*). In particular, for both observed and modeled CA and IO currents at positive voltages, membrane depolarization decreases the fast time constant of inactivation and increases the slow time constant of inactivation. This behavior is expected when the C↔O equilibrium is weakly voltage dependent and the channels undergo closed-state inactivation from the preopen closed state (Klemic et al., 1998). With moderate depolarizations, channel closing is significant, and, consequently, preferential closed-state inactivation from $C_4$ is favorable. Stronger depolarizations favor channel opening, which slows closed-state inactivation ($\tau_{SLOW}$ increases) by reducing the occupancy of $C_4$, and open-state inactivation appears somewhat faster ($\tau_{FAST}$ decreases). Because the modeled rates of open- and closed-state inactivation are similar for channels in IO patches (Table 3) the fast time constant of inactivation in this case is also partly determined by closed-state inactivation. Consequently, the relative weight of the slow component from IO patches is decreased (Figs. 3 and 10). Supporting the relation between the hyperpolarizing shift of the prepulse steady-state inactivation curve and accelerated closed-state inactivation, the model also faithfully reproduces this behavior when the C→I transition is assumed 2.5 times faster

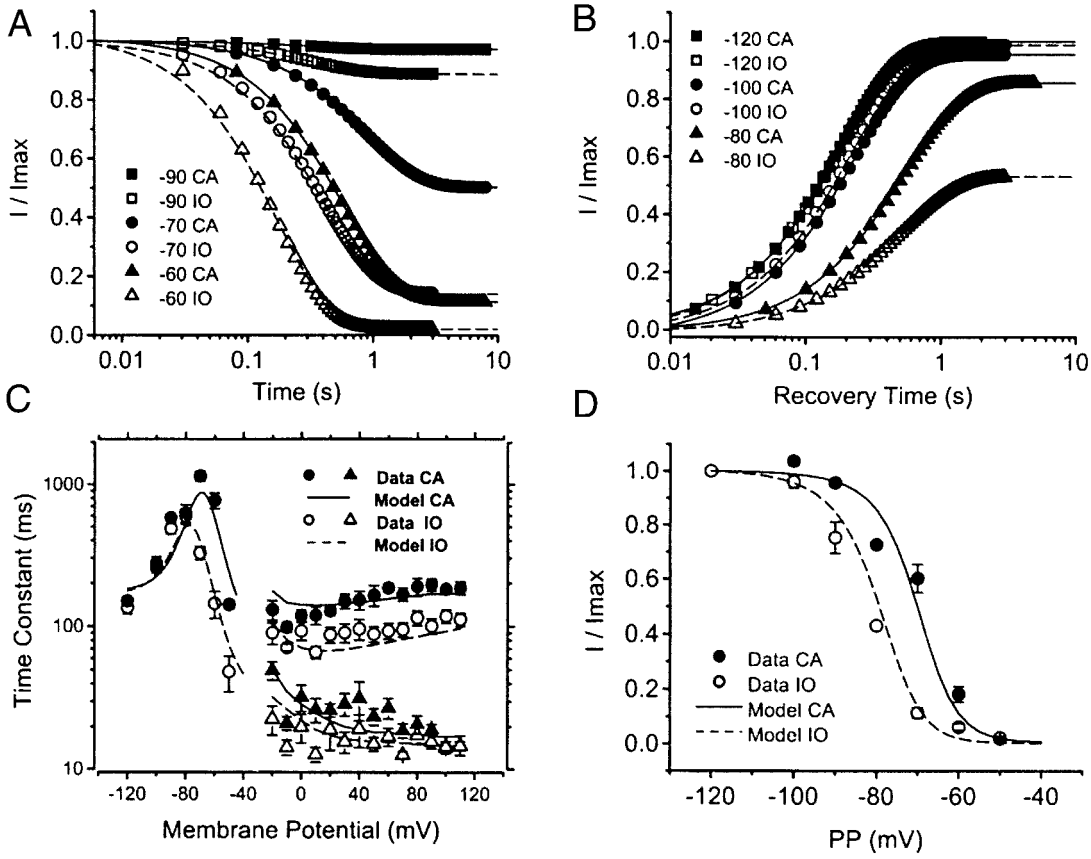


FIGURE 11 Simulations generated from Scheme 1 (inactivation). All simulations shown here attempt to model the average behavior of Kv4.1 channels expressed in *Xenopus* oocyte macropatches (CA and IO). The parameters used for these simulations are shown in Table 3. (*A*) Simulated time courses of the development of inactivation at negative membrane potentials (for pulse protocol, Fig. 4, *legend*). (*B*) Simulated time courses of the recovery from inactivation at hyperpolarized voltages (for pulse protocol, Fig. 5, *legend*). Solid lines in (*A*) and (*B*) are the best exponential fits. (*C*) Voltage dependence of the compiled time constants extracted from the observations (symbols replotted from Figs. 3–5) and from the simulated currents (*lines*). (*D*) Observed (*symbols* from Fig. 6, panel (*F*)) and simulated (*lines*) steady-state prepulse inactivation. Using the parameters in Table 3, the simulated curves resulted from computing the equilibrium probabilities that the channels are not inactivated at the indicated membrane potentials. The modeled behavior in panels (*C*) and (*D*) closely describes the observations.

in IO patches (Fig. 11, *A* and *D*). Also, as expected and in a manner that is independent of patch configuration, observed and modeled currents exhibit fast exponential recovery from inactivation at hyperpolarized voltages (−120 to −90 mV; Fig. 11 *B*). To refine the simulations of Kv4 gating in IO patches, the voltage-dependent deactivation rate ($\beta$) was slowed by ~50%, and the closing rate was increased by 10% (Table 3). Conservatively, the latter takes into account the possibility that channel closing is also accelerated in IO patches.

Accelerated tail current relaxations were observed when macroscopic inactivation was significantly accelerated in IO patches (Fig. 7). However, that trend was not statistically significant. Nevertheless, faster channel closing in IO patches underscores the significance of the inactivation pathway from closed state in Kv4 channels. If channels undergo more favorable closed-state inactivation according to Scheme 1, faster channel closing could contribute further to a faster development of inactivation, because the speed of slow inactivation depends on the occupancy of the preopen inactivation-permissive closed state.

At a first glance, Kv4.3 exhibits changes upon patch excision that seemed different from those observed with Kv4.1. Whereas patch excision mainly affected the slow component of inactivation in Kv4.1, the fast component in Kv4.3 underwent the most significant change (Figs. 3 and 9). It is important to note, however, that the fast component is already dominant in CA patches expressing Kv4.2 and Kv4.3 channels or whole-cell currents mediated by these channels. Therefore, Kv4.2 and Kv4.3 appear to inactivate faster than Kv4.1 at positive voltages, in spite of the fact that the observed rate of closed-state inactivation of Kv4.3 at negative voltages was significantly slower compared to that of Kv4.1 (Figs. 4 and 9). Scheme 1 can explain these differences without altering the conclusions regarding preferential modulation of closed-state inactivation in all Kv4

**TABLE 3 Parameters of the simulations assuming that Scheme 1 models Kv4.1 gating**

| Parameter* | Cell-Attached | Inside-Out | Fold-change |
|---|---|---|---|
| $\alpha$ ($s^{-1}$) | 300 | 300 | 0 |
| $\beta$ ($s^{-1}$) | 1.9 | 1.2 | 1.5 |
| $V_\alpha$ (mV) | 28 | 28 | 0 |
| $V_\beta$ (mV) | 16 | 16 | 0 |
| $k_{co}$ ($s^{-1}$) | 400 | 400 | 0 |
| $k_{oc}$ ($s^{-1}$) | 450 | 500 | 1.1 |
| $V_{co}$ (mV) | 380 | 380 | 0 |
| $V_{oc}$ (mV) | 175 | 175 | 0 |
| $k_{oi}$ ($s^{-1}$) | 70 | 70 | 0 |
| $k_{io}$ ($s^{-1}$) | 70 | 70 | 0 |
| $k_{ci}$ ($s^{-1}$) | 22 | 56 | 2.5 |
| $k_{ic}$ ($s^{-1}$) | 0.05 | 0.05 | 0 |
| $k_{56}$ ($s^{-1}$) | 12 | 12 | 0 |
| $k_{65}$ ($s^{-1}$) | 12 | 12 | 0 |
| $f$ (allosteric factor) | 0.31 | 0.31 | 0 |

*Scheme 1 assumes that the transitions between closed states and the opening step are governed by rate constants that depend exponentially on membrane potential. Accordingly, $\alpha$, $\beta$, $k_{co}$, and $k_{oc}$ are the rates in the absence of membrane potential ($V = 0$); and $V_\alpha$, $V_\beta$, $V_{co}$, and $V_{oc}$ are the corresponding voltage sensitivities. The computed equivalent gating charges are 10 $e_0$ from all the closed state transitions, and 0-.2 $e_0$ from the opening step.

channels. The main assumptions are that rapid open-state inactivation is more stable in Kv4.2 and Kv4.3 channels, and that the nearly absorbing inactivated state in all Kv4 channels is that originating from the preopen closed state. Simulations of macroscopic Kv4.2 and Kv4.3 currents demonstrated that both slow and fast phases of inactivation depend on the rate of close-state inactivation. In agreement with the data, increasing this rate primarily accelerates the fast phase of the current at positive voltages and the development of inactivation at negative voltages.

## Limitations of the kinetic analysis and the allosteric model

The model simulations generated from Scheme 1 closely reproduce the main functional features of all Kv4 channels and the most significant kinetic changes induced by patch excision (Figs. 10 and 11). However, in spite of the reasonable success of Scheme 1, some significant discrepancies between observed and modeled currents were seen when comparing the kinetics of current activation and tail current relaxations at low voltages. Relative to the observed currents, the modeled currents tend to rise more slowly (Figs. 2 and 10; −40 to 0 mV); and the modeled difference between the times-to-peak from currents in CA and IO patches (as a result of faster inactivation) was qualitatively similar (Fig. 3 *A*) but systematically smaller than the observed one (at various membrane potentials, the observed difference ranged between 20 and 50%, and the modeled difference ranged between 11 and 24%). Even though all observed and modeled tail current relaxations were biexponential, the modeled ones differed more significantly from the observations, between −70 and −50 mV (Figs. 7 and 10). Given these observations, the current results and analysis cannot completely rule out altered activation gating in IO patches. Additional studies will be necessary to solve these discrepancies and further constrain the analysis of the proposed allosteric model. For instance, more information is needed on single-channel kinetics and the contribution of subconductance levels to the kinetics of macroscopic currents. The presence of subconductance levels that contribute to the complex kinetics of single Kv4 currents was recently documented (Jerng et al., 1999), but a more detailed analysis of their amplitude and occurrence is not yet available. Also, voltage-dependent gating of Kv4 channels is not well characterized (e.g., gating currents).

## Molecular mechanisms of inactivation and putative modulatory factors

The analysis discussed above demonstrated that closed-state inactivation is a significant pathway of inactivation gating in Kv4 channels and an important functional target of modulatory mechanisms. What is the molecular basis of this modulation? A plausible inactivation site that is directly or allosterically modulated might be located at the internal vestibule of the channel in Kv4 channels. Important components of this region include the lower section of the S6 segment and the S4–S5 loop, which have been shown to contribute to channel closing and closed-state inactivation in Kv4 channels (Jerng et al., 1999). The nature of the factor(s) that modulate inactivation gating of these channels has, however, remained elusive. In preliminary experiments, we have examined various putative regulatory factors. Oxidation of the channel protein is not likely to be involved because bathing the cytoplasmic side of the patch with glutathione (5 mM) was not able to reverse or prevent the kinetic changes induced by patch excision. Furthermore, supplementing the intracellular solution with various second-messenger molecules (ATP, PIP2, or GTP-γ-S) does not influence these changes significantly. Also, agents that disrupt cytoskeletal structures (colchicine and nocodazol) were unable to systematically favor faster inactivation of Kv4.1. In contrast, modulation of inactivation gating in voltage-gated $Na^+$ channels has been associated with the cytoskeleton and its contribution to the mechanical stability of the membrane (Shcherbatko et al., 1999).

A recent discovery showed that certain $Ca^{2+}$-binding proteins (dubbed KChIP for $K^+$ channel interacting protein) selectively modulate the expression level and inactivation gating of Kv4 channels (An et al., 2000). In preliminary coexpression experiments, we also found that, although Kv4.1 and Kv4.3 channels exhibit novel inactivation properties in the presence of KChIP-1, the observed rate of inactivation was enhanced upon patch excision in a manner analogous to that observed in the absence of KChIP-1 (E. J.

Beck and M. Covarrubias, unpublished). This result suggests that the modulation of closed-state inactivation reported here is not affected by the interaction of Kv4 channels with KChIP.

In determining the nature of the factor(s) that modulate closed-state inactivation in Kv4 channels, it is important to consider that the kinetic changes induced by patch excision are relatively rapid, time-dependent, and reversible upon patch cramming. These results suggest that a putative modulator is readily available in the oocyte's cytoplasm and that its effective concentration changes as it rapidly diffuses away (IO patches) or reaches the cytoplasmic side of the channel (crammed patches). Thus, it does not interact tightly with the channel protein (as might be expected for a specific regulatory subunit). The putative cytoplasmic modulator may favor closed-state inactivation by a direct weak interaction or by controlling the balance between opposing enzymatic activities (kinase/phosphatase) that modify gating of the channel. Further research is necessary to determine all the factors and pathways involved in the modulation of Kv4 inactivation gating. A possible clue arises from the relationship between the modulation of closed-state inactivation described here and a similar modulation observed when Kv4 channels were coexpressed with factors encoded by the low-molecular-weight mRNA from brain (Chabala et al., 1993; Serodio et al., 1994, 1996). Such factors might also induce more favorable closed-state inactivation in intact oocytes by enzymatically removing a modulator normally present in *Xenopus* oocytes.

### The physiological significance of closed-state inactivation in Kv4 channels

The gating mechanism and modulation of Kv4 channels described here underscores the importance of closed-state inactivation in controlling the function of these channels over a broad range of relevant membrane potentials. Because the opening step does not appear to be strongly favored in Kv4 channels and the preopen closed state is inactivation permissive, closed-state inactivation is significant even at membrane potentials that activate a significant fraction of channels (0 to +100 mV). Consequently, the open probability of these channels is probably low, and the development of inactivation of macroscopic outward currents under physiological conditions is significantly determined by closed-state inactivation. This property renders Kv4 channels well suited to regulate electrical excitability in the subthreshold range of membrane potentials and to shape the action potential without aborting it. During the after-hyperpolarization that follows an action potential Kv4 channels rapidly recover from inactivation. The subsequent slow depolarization causes them to activate and inactivate. Thus, the magnitude and time course (i.e., the development of inactivation) of the evoked Kv4 current can determine the slope and magnitude of the slow depolarization before reaching the action potential threshold, and, consequently, the interspike interval. This mechanism controls slow repetitive spike firing in neurons (Connor and Stevens, 1971; Connors, 1978). If the interspike depolarization does not inactivate the Kv4 channels completely, the remaining channels might activate during the action potential, and the outward current generated by these channels could also help to shape the repolarizing phase of the action potential in a way that may depend on the time course of inactivation (e.g., cardiac action potentials). Clearly, all these physiological actions can be strongly influenced by modulation of closed-state inactivation in Kv4 channels, which, in turn, can affect signaling in the brain and the contractility of the heart.

We thank Mr. Thanawath Harris for harvesting and preparing *Xenopus* oocytes and Dr. Mohammad Shahidullah for providing additional data for Fig. 8 *D* and examining the effects of patch excision on Kv4.2 currents. Also, we thank Drs. Richard Horn and Michael O'Leary for critically reading earlier versions of this manuscript.

This study constitutes part of E. J. Beck's doctoral thesis. The work was supported by National Institutes of Health grant R01 NS32337 (M.C.). E. J. Beck was supported by a departmental National Institutes of Health training grant AA07463.

## REFERENCES

An, W. F., M. R. Bowlby, M. Betty, J. Cao, H. P. Ling, G. Mendoza, J. W. Hinson, K. I. Mattsson, B. W. Strassle, J. S. Trimmer, and K. J. Rhodes. 2000. Modulation of A-type potassium channels by a family of calcium sensors. *Nature.* 403:553–556.

Antz, C., T. Bauer, H. Kalbacher, R. Frank, M. Covarrubias, H. R. Kalbitzer, J. P. Ruppersberg, T. Baukrowitz, and B. Fakler. 1999. Control of $K^+$ channel gating by protein phosphorylation: structural switches of the inactivation gate. *Nat. Struct. Biol.* 6:146–150.

Ayer R. K., Jr., and F. J. Sigworth. 1997. Enhanced closed-state inactivation in a mutant Shaker $K^+$ channel. *J. Membr. Biol.* 157:215–230.

Beck, E. J., M. R. Bowlby, W. F. An, K. J. Rhodes, and M. Covarrubias. 2001. Modulation of Kv4 inactivation gating by a calcium binding protein KChIP-1. *Biophys. J.* 80:439.A.

Beck, E. J., and M. Covarrubias. 1999. Modulation of slow inactivation gating in Kv4.1 $K^+$ channels. *Biophys. J.* 76:414.A

Beck, E. J., and M. Covarrubias. 2000. Selective modulation of closed-state inactivation in inside-out membrane patches expressing Kv4.1 channels. *Biophys. J.* 78:212.A.

Beck, E. J., R. G. Sorensen, S. J. Slater, and M. Covarrubias. 1998. Interactions between multiple phosphorylation sites in the inactivation particle of a $K^+$ channel. Insights into the molecular mechanism of protein kinase C action. *J. Gen. Physiol.* 112:71–84.

Campbell, D. L., R. L. Rasmusson, Q. Yusheng, and H. C. Strauss. 1993. The calcium-independent transient outward potassium current in isolated ferret ventricular myocytes. *J. Gen. Physiol.* 101:571–601.

Chabala, L. D., N. Bakry, and M. Covarrubias. 1993. Low molecular weight poly(A)+ mRNA species encode factors that modulate gating of a non-Shaker A-type $K^+$ channel. *J. Gen. Physiol.* 102:713–728.

Connor, J. A. 1978. Slow repetitive activity from fast conductance changes in neurons. *Fed. Proc.* 37:2139–2145.

Connor, J. A., and C. F. Stevens. 1971. Voltage clamp studies of a transient outward membrane current in gastropod neural somata. *J. Physiol. (Lond.).* 213:21–30.

Costantin, J. L., N. Qin, M. N. Waxham, L. Birnbaumer, and E. Stefani. 1999. Complete reversal of run-down in rabbit cardiac $Ca^{2+}$ channels by

patch-cramming in *Xenopus* oocytes: partial reversal by protein kinase A. *Pfluegers Arch. Eur. J. Physiol.* 437:888–894.

Covarrubias, M., A. Wei, L. Salkoff, and T. Vyas. 1994. Elimination of rapid potassium channel inactivation by phosphorylation of the inactivation gate. *Neuron.* 13:1403–1412.

Dixon, J. E., W. Shi, H. S. Wang, C. McDonald, H. Yu, R. S. Wymore, I. S. Cohen, and D. McKinnon. 1996. Role of the Kv4.3 $K^+$ channel in ventricular muscle. A molecular correlate for the transient outward current. *Circ. Res.* 79:659–668.

Drain, P., A. E. Dubin, and R. W. Aldrich. 1994. Regulation of Shaker $K^+$ channel inactivation gating by the cAMP-dependent protein kinase. *Neuron.* 12:1097–1109.

Hoffman, D. A., J. C. Magee, C. M. Colbert, and D. Johnston. 1997. $K^+$ channel regulation of signal propagation in dendrites of hippocampal pyramidal neurons. *Nature.* 387:869–875.

Jegla, T., and L. Salkoff. 1997. A novel subunit for shal $K^+$ channels radically alters activation and inactivation. *J. Neurosci.* 17:32–44.

Jerng, H. H., and M. Covarrubias. 1997. $K^+$ channel inactivation mediated by the concerted action of the cytoplasmic N- and C-terminal domains. *Biophys. J.* 72:163–174.

Jerng, H. H., M. Shahidullah, and M. Covarrubias. 1999. Inactivation gating of Kv4 potassium channels: molecular interactions involving the inner vestibule of the pore. *J. Gen. Physiol.* 113:641–660.

Johns, D. C., H. B. Nuss, and E. Marban. 1997. Suppression of neuronal and cardiac transient outward currents by viral gene transfer of dominant-negative Kv4.2 constructs. *J. Biol. Chem.* 272:31598–31603.

Kirichok, Y. V., A. V. Nikolaev, and O. A. Krishtal. 1998. [$K^+$] out accelerates inactivation of Shal-channels responsible for A-current in rat CA1 neurons. *Neuroreport.* 9:625–629.

Klemic, K., C.-C. Shieh, G. Kirsch, and S. W. Jones. 1998. Inactivation of Kv2.1 channels. *Biophys. J.* 77:1945–1959.

Kuo, C. C., and B. P. Bean. 1994. $Na^+$ channels must deactivate to recover from inactivation. *Neuron.* 12:819–829.

Kramer, J. W., M. A. Post, A. M. Brown, and G. E. Kirsch. 1998. Modulation of potassium channel gating by coexpression of Kv2.1 with regulatory Kv5.1 or Kv6.1 alpha-subunits. *Am. J. Physiol.* 274:1–10.

Kramer, R. H. 1990. Patch cramming: monitoring intracellular messengers in intact cells with membrane patches containing detector ion channels. *Neuron.* 4:335–341.

Kupper, J., M. R. Bowlby, S. Marom, and I. B. Levitan. 1995. Intracellular and extracellular amino acids that influence C-type inactivation and its modulation in a voltage-dependent potassium channel. *Pfluegers Arch. Eur. J. Physiol.* 430:1–11.

Malin, S. A., and J. M. Nerbonne. 2000. Elimination of the fast transient in superior cervical ganglion neurons with expression of KV4.2W362F: molecular dissection of $I_A$. *J. Neurosci.* 20:5191–5199.

Olcese, R., R. Latorre, L. Toro, F. Bezanilla, and E. Stefani. 1997. Correlation between charge movement and ionic current during slow inactivation in Shaker $K^+$ channels. *J. Gen. Physiol.* 110:579–589.

Petersen, K. R., and J. M. Nerbonne. 1999. Expression environment determines $K^+$ current properties: Kv1 and Kv4 alpha-subunit-induced $K^+$ currents in mammalian cell lines and cardiac myocytes. *Pfluegers Arch. Eur. J. Physiol.* 437:381–392.

Pongs, O., T. Leicher, M. Berger, J. Roeper, R. Baehring, D. Wray, K P. Giese, A. J. Silva, and J. F Storm. 1999. Functional and molecular aspects of voltage-gated $K^+$ channel $\beta$ subunits. *Ann. NY Acad. Sci.* 868:344–355.

Rettig, J., S. H. Heinemann, F. Wunder, C. Lorra, D. N. Parcej, J. O. Dolly, and O. Pongs. 1994. Inactivation properties of voltage-gated $K^+$ channels altered by presence of beta-subunit. *Nature.* 369:289–294.

Roeper, J., C. Lorra, and O. Pongs. 1997. Frequency-dependent inactivation of mammalian A-type $K^+$ channel Kv1.4 regulated by $Ca^{2+}$/calmodulin-dependent protein kinase. *J. Neurosci.* 17:3379–3391.

Ruppersberg, J. P., M. Stocker, O. Pongs, S. H. Heinemann, R. Frank, and M. Koenen. 1991. Regulation of fast inactivation of cloned mammalian $I_K$(A) channels by cysteine oxidation. *Nature.* 352:711–714.

Serodio, P., C. Kentros, and B. Rudy. 1994. Identification of molecular components of A-type channels activating at subthreshold potentials. *J. Neurophysiol.* 72:1516–1529.

Serodio, P., D. M. Vega-Saenz, and B. Rudy. 1996. Cloning of a novel component of A-type $K^+$ channels operating at subthreshold potentials with unique expression in heart and brain. *J. Neurophysiol.* 75: 2174–2179.

Shcherbatko, A., F. Ono, G. Mandel, and P. Brehm. 1999. Voltage-dependent sodium channel function is regulated through membrane mechanics. *Biophys. J.* 77:1945–1959.

Shibata, R., K. Nakahira, K. Shibasaki, Y. Wakazono, K. Imoto, and K. Ikenaka. 2000. A-type $K^+$ current mediated by the Kv4 channel regulates the generation of action potential in developing cerebellar granule cells. *J. Neurosci.* 20:4145–4155.

Smith-Maxwell, C. J., J. L. Ledwell, and R. W. Aldrich. 1998. Uncharged S4 residues and cooperativity in voltage-dependent potassium channel activation. *J. Gen. Physiol.* 111:421–439.

Solc, C. K., and R. W. Aldrich. 1990. Gating of single non-Shaker A-type potassium channels in larval *Drosophila* neurons. *J. Gen. Physiol.* 96: 135–165.

Song, W. J., T. Tkatch, G. Baranauskas, N. Ichinohe, S. T. Kitai, and D. J. Surmeier. 1998. Somatodendritic depolarization-activated potassium currents in rat neostriatal cholinergic interneurons are predominantly of the A type and attributable to coexpression of Kv4.2 and Kv4.1 subunits. *J. Neurosci.* 18:3124–3137.